Distribution and Activity of Mitochondrial Proteins in Vascular and Avascular Retinas: Implications for Retinal Metabolism

Glyn Chidlow, John P. M. Wood, Paul I. Sia, and Robert J. Casson

Ophthalmic Research Laboratories, Discipline of Ophthalmology and Visual Sciences, University of Adelaide, Adelaide, South Australia, Australia

PURPOSE. Understanding the energetics of retinal neurons and glia is crucial for developing therapies for diseases that feature deficits in nutrient or oxygen availability. Herein, we performed a detailed characterization of the distribution and activity of mitochondrial proteins in the vascularized retinas of rat and marmoset, and the avascular retinas of rabbit and guinea pig. Further, we delineated expression of ubiquitous mitochondrial creatine kinase (uMtCK).

METHODS. Expression of eight mitochondrial proteins was investigated using Western blotting, single- and double-labeling immunohistochemistry. Activities of cytochrome c oxidase, succinate dehydrgogenase, and isocitrate dehydrogenase were determined by enzyme histochemistry using unfixed tissue sections.

RESULTS. In vascularized retinas, immunoreactivities were characterized by strong, punctate labeling in the plexiform layers, photoreceptor inner segments, somas of various cell types, notably retinal ganglion cells (RGCs), and the basolateral surface of the retinal pigment epithelium. In avascular retinas, immunoreactivities featured intense labeling of inner segments, together with weak, but unambiguous, staining of both plexiform layers. RGCs were relatively enriched. In Müller cells of avascular retinas, mitochondria were restricted to scleral-end processes. For each species, enzyme activity assays yielded similar results to the protein distributions. Labeling for uMtCK in vascular and avascular retinas was fundamentally similar, being restricted to neuronal populations, most notably inner segments and RGCs. Of all of the mitochondrial proteins, uMtCK displayed the strongest labeling in avascular retinas. uMtCK was not detectable in Müller cells in any species.

CONCLUSIONS. The current findings advance our understanding of the metabolic similarities and differences between vascular and avascular retinas.

Keywords: retina, mitochondria, avascular, vascular, aerobic metabolism, mitochondrial creatine kinase

The retina has prodigious energy demands in order to meet the needs of phototransduction and neurotransmission. As a consequence, retinal oxygen[1] and glucose[2] consumption is exceptionally high relative to other tissues. In the majority of mammals, the retina is served by a dual blood supply, comprising the choroidal circulation that supplies the photoreceptors, and the retinal circulation.[3] The retinal circulation serves the inner retina and is divided into the following two capillary beds: a superficial plexus located within the nerve fiber/ganglion cell layers, and a deeper plexus in the inner nuclear and outer plexiform layers. In certain mammals, however, the retinal circulation is either highly restricted or is completely absent.[4] In the rabbit, retinal vessels are confined to a superficial network of capillaries lying within the medullary rays—a central band of myelinated nerve fibers, while the guinea pig retina is completely devoid of vessels. In these species, the choroidal blood supply is essentially responsible for oxygen and nutrient delivery to the entire retina. Avascular retinas are markedly thinner than vascular retinas, presumably to aid diffusion of oxygen and nutrients; yet, sophisticated modelling by Yu and Cringle[5,6] has demonstrated that oxygen tension within most layers of these retinas is still exceptionally low; photoreceptor inner segments consume the overwhelming majority of oxygen supplied by the choroid.

It has been proposed that cells located farthest from the choroid must display metabolic adaptations to surmount the constraints imposed by low oxygen availability.[7] Indeed, it is frequently asserted that the inner layers of wholly or predominantly avascular retinas are devoid of mitochondria.[8] This rational assumption is based largely upon the results of a single study,[9] which failed to identify cytochrome c oxidase (COX) immunolabeling in the inner layers of the guinea pig retina. Yet, earlier work by Germer and colleagues,[10,11] and a subsequent report by Stone et al.,[12] demonstrated that mitochondria are present in the inner retina—notably within retinal ganglion cells (RGCs). Nevertheless, immunoreactivity for COX was sparse in the inner layers of both guinea pig and rabbit retinas, prompting the authors to postulate that expression of COX is downregulated in these mitochondria.[12] Surprisingly, there have been no systematic investigations of the

331

Investigative Ophthalmology & Visual Science

expression of key mitochondrial proteins in avascular retinas, nor have mitochondrial enzyme activities been studied by enzyme histochemistry using tissue sections. Importantly, there is also little known about the distribution of ubiquitous mitochondrial creatine kinase (uMtCK) in vascular and avascular retinas. UMtCK, which is bound to the outer surface of the inner mitochondrial membrane, converts creatine to the high-energy compound phosphocreatine, providing energy buffering in cells with variable energy requirements.[13] UMtCK facilitates the accretion of a diffusible, cellular energy buffer in the form of a phosphocreatine store that is used to regenerate ATP when demand is high. In recent years, there has been increasing recognition of the importance of the creatine/phosphocreatine pathway in energy metabolism within the central nervous system.[14] UMtCK has been shown to be abundantly expressed in neurons with high oxidative demand.[15] The presence of uMtCK within the inner layers of avascular retinas would support the notion of the functional relevance of these mitochondria.

Understanding the energetics of the various neuronal and glial classes of the retina is of fundamental importance in the development of therapeutic strategies for retinal diseases that feature deficits in nutrient or oxygen availability. The aim of the present study was to perform a detailed characterization of the distribution and activity of mitochondrial proteins in the vascularized retinas of rat and common marmoset as well as in the avascular retinas of rabbit and guinea pig. Further, we sought to delineate the expression of uMtCK in each species. To achieve these goals, we employed a combination of Western blotting and immunohistochemistry using well-characterized antibodies, together with enzyme histochemistry assays.

MATERIALS AND METHODS

Animals and Tissue Processing

This study was approved by the SA Pathology/Central Heath Network (CHN) Animal Ethics Committee (Adelaide, Australia) and conformed with the Australian Code of Practice for the Care and Use of Animals for Scientific Purposes, 2013, and with the ARVO Statement for the Use of Animals in Ophthalmic and Vision Research. Adult Sprague-Dawley rats (~250 g) and BALB/C mice were housed in a temperature- and humidity-controlled room with a 12-hour light/dark cycle and were provided with food and water ad libitum. Following ethical approval from the SA Pathology/CHN Animal Ethics Committee, we were able to obtain ocular tissue from adult marmosets (*Callithrix jacchus*), aged 10 to 14 years, belonging to the colony housed at the Queen Elizabeth Hospital (South Australia, Australia) that were being euthanized.[16] We are grateful to Toby Coates for participating in this tissue sharing initiative, which has obvious benefits from an ethical perspective. Following ethical approval from the University of South Australia Animal Ethics Committee (Adelaide, Australia), we obtained ocular tissue from adult guinea pigs that were excess stock from a breeding colony and were being euthanized. Ocular tissue from adult pigmented (Havana) and albino (New Zealand White) rabbits was obtained from a local supplier at the time of euthanasia. The number of eyes of each species used in the study was as follows: immunohistochemistry: rat (n = 6), marmoset (n = 3), rabbit (n = 6, comprising n = 3 albino and n = 3 pigmented), guinea pig (n = 3), and mouse (n = 3); Western blotting: rat (n = 3), marmoset (n = 2), rabbit (n = 4, comprising n = 2 albino and n = 2 pigmented), and guinea pig (n = 2); and enzyme histochemistry: rat (n = 3), rabbit (n = 4, comprising n = 2 albino and n = 2 pigmented), and guinea pig (n = 2).

There was no consistent orientation of globes with regard to the nasal-temporal, superior-inferior quadrants of the retina analyzed. Sections were typically taken at the level of the optic nerve head and hence comprise at least two quadrants. We cannot categorically rule out expression differences between different regions of the retina in any species; however, no such differences were apparent in any of our examinations. Globes that were used for immunohistochemistry were immersion-fixed in 10% buffered formalin or Davidson's solution for 24 (rat) or 48 hours (for the larger guinea pig, rabbit, and marmoset eyes), and transferred to 70% ethanol until processing. Davidson's solution, which comprises two parts formaldehyde (37%), three parts 100% ethanol, one part glacial acetic acid, and three parts water, is the preferred fixative for whole eyes as it provides optimal tissue morphology while avoiding retinal detachment. Rat eyes were placed into fixative within 15 minutes of euthanasia. Marmoset, rabbit, and guinea pig eyes were placed into fixative approximately 30 minutes after euthanasia. Eyes were then processed for routine paraffin-embedded sections. Globes were embedded sagittally. In all cases, 4-μm sections were cut.

Immunohistochemistry

Colorimetric immunohistochemistry was performed as previously described.[17–19] In brief, tissue sections were deparaffinized, endogenous peroxidase activity was blocked, and high-temperature antigen retrieval was performed. Subsequently, sections were incubated in the primary antibody (Table 1), followed by consecutive incubations with biotinylated secondary antibody and streptavidin-peroxidase conjugate. Color development was achieved using 3,3′-diaminobenzidine.

For double-labeling fluorescent immunohistochemistry, visualization of one antigen was achieved using a three-step procedure (primary antibody, biotinylated secondary antibody, streptavidin-conjugated AlexaFluor 488 or 594), while the second antigen was labeled by a two-step procedure (primary antibody, secondary antibody conjugated to AlexaFluor 488 or 594). Sections were prepared as above, then incubated overnight at room temperature in the appropriate combination of primary antibodies. On the following day, sections were incubated with the appropriate biotinylated secondary antibody for the three-step procedure plus the correct secondary antibody conjugated to AlexaFluor 488 or 594 for the two-step procedure, followed by streptavidin-conjugated AlexaFluor 488 or 594. Sections were then mounted using antifade-mounting medium and examined under a confocal fluorescence microscope or an epifluorescent microscope equipped with a scientific grade, cooled charged-coupled device camera. Confocal microscopy eliminates out of focus light, whereas wide-field epifluorescent microscopy does not; however, for very thin specimens (<5 μm in thickness), wide-field images capture an accurate representation of the light emitted, because there is minimal out-of-focus structure to contaminate it.[20] In this study, both microscopes yielded analogous images of the double-labeling fluorescent immunohistochemistry.

Confirmation of the specificity of antibody labeling was judged by the morphology and distribution of the labeled cells, by the absence of signal when the primary antibody was replaced by isotype/serum controls, by comparison with the expected staining pattern based on our own, and other, previously published results, and by the detection within retinal samples of a protein at the expected molecular weight by Western blotting. The relative mitochondrial labeling intensities in the different retinal layers were assessed and

TABLE 1. Primary Antibodies Used in the Study

Protein	Source	Clone/Cat. No.	Species	Immunogen	Dilution
Actin	Sigma, Castle Hill, New South Wales, Australia	Clone AC-15	Mouse	Slightly modified β-cytoplasmic actin N-terminal peptide	1:20,000*
CD31	Dianova, Hamburg, Germany	Clone SZ31	Rat	Murine amino acid fragment to CD31	1:500
uMtCK	Proteintech, Rosemont, IL, USA	Cat# 15346-1-AP	Rabbit	CKMT1A fusion protein Ag7583	1:750† 1:5000 1:10,000*
Cytochrome c	Santa-Cruz Biotechnology, Dallas, TX, USA	Cat# sc-8385	Goat	Peptide mapping at the C-terminus of cytochrome c of human origin	1:1000 1:1000*
Cytochrome c oxidase Subunit IV	Molecular Probes, Thermo Fisher Scientific, Waltham, MA, USA	Clone 20E8C12	Mouse	Bovine Complex IV (native holoenzyme protein, purified from liver	1:10,000 1:2500*
Glutamate dehydrogenase	Cell Signaling Technology, Danvers, MA, USA	Cat# 12793	Rabbit	Synthetic peptide corresponding to residues surrounding Pro190 of human glutamate dehydrogenase 1 protein	1:1000
Heat shock protein 60	Enzo Lifesciences, Farmingdale, NY, USA	Cat# ADI-SPA-807	Mouse	Recombinant human HSP60	1:1000 1:1000*
Mitochondrial pyruvate carrier 1	Cell Signaling Technology	Cat# 14462	Rabbit	synthetic peptide corresponding to residues near the carboxy terminus of human MPC1 protein	1:1000 1:1000*
Myelin basic protein	Dako, Sydney, New South Wales, Australia	Cat# A0623	Rabbit	Myelin basic protein isolated from human brain	1:600†
Pyruvate dehydrogenase	Cell Signaling Technology	Cat# 3205	Rabbit	Synthetic peptide corresponding to the sequence of human pyruvate dehydrogenase	1:500 1:1000*
RBPMS	Merck-Millipore, Bayswater, Victoria, Australia	Cat# ABN1362	Rabbit	KLH-conjugated linear peptide corresponding to a sequence from the N-terminal region of human RBPMS	1:200†
S100	Dako	Cat# Z0311	Rabbit	S100 isolated from cow brain	1:1500†
SOD-2	Antibody Technology Australia Pty Ltd, Adelaide, South Australia, Australia	Cat# SOD2R	Rabbit	human/rat/mouse SOD2 aa. 25-43	1:10,000 1:10,000*
Synaptophysin	Roche Diagnostics, North Ryde, New South Wales, Australia	Clone SY 38	Mouse	Vesicular fraction of bovine brain	50 ng/mL

* Dilution used for Western blotting.
† Dilution used for two-step fluorescent immunostaining procedure.

visually scored on a qualitative scale from '−' (no staining detected) to '+++' (intense staining).

Histochemical Analysis of Mitochondrial Enzyme Activities

Assessment of COX, succinate dehydrogenase (SDH), and isocitrate dehydrogenase (ICDH) activities in situ were determined using enzyme histochemistry assays. Eyes from adult rats, rabbits or guinea pigs were enucleated and dissected into eyecups. They were then snap frozen in liquid nitrogen or in dry ice-cooled isopentane and stored at −80°C until use. Frozen, unfixed vertical sections (9 μm) were taken, air dried, and used immediately in enzyme assays.

For COX, tissue sections were incubated for 40 minutes at 37°C in a reaction medium containing 5 mg 3,3′-diamino-benzidine, 10 mg of cytochrome c, 60 μg/mL catalase, and 4% sucrose in 10 mL 0.0 5M phosphate buffer (pH 7.4). For

SDH, tissue sections were incubated for 30 minutes at 37°C in a reaction medium containing (final concentrations) 100 mM sodium succinate, 3 mM nitro blue tetrazolium, 0.25 mM phenazine methosulphate, and 1 mM sodium azide in 0.2M Tris-HCl buffer containing 11% polyvinyl alcohol (pH 7.4). For ICDH, tissue sections were incubated for 20 minutes at 37°C in a reaction medium containing (final concentrations) 100 mM sodium isocitrate, 5 mM β-nicotinamide adenine dinucleotide, 10 mM $MgCl_2$, 5 mM nitro blue tetrazolium, 0.25 mM phenazine methosulphate, and 10 mM sodium azide in 0.2 M Tris-HCl buffer containing 22% polyvinyl alcohol (pH 7.4). To terminate each reaction, sections were rinsed in distilled water, fixed for 5 minutes in neutral buffered formalin, and mounted using aqueous mounting medium. Negative control slides, which were processed simultaneously, were performed in the absence of substrate and yielded negligible reaction product. The relative mitochondrial activity intensities in the different retinal layers were
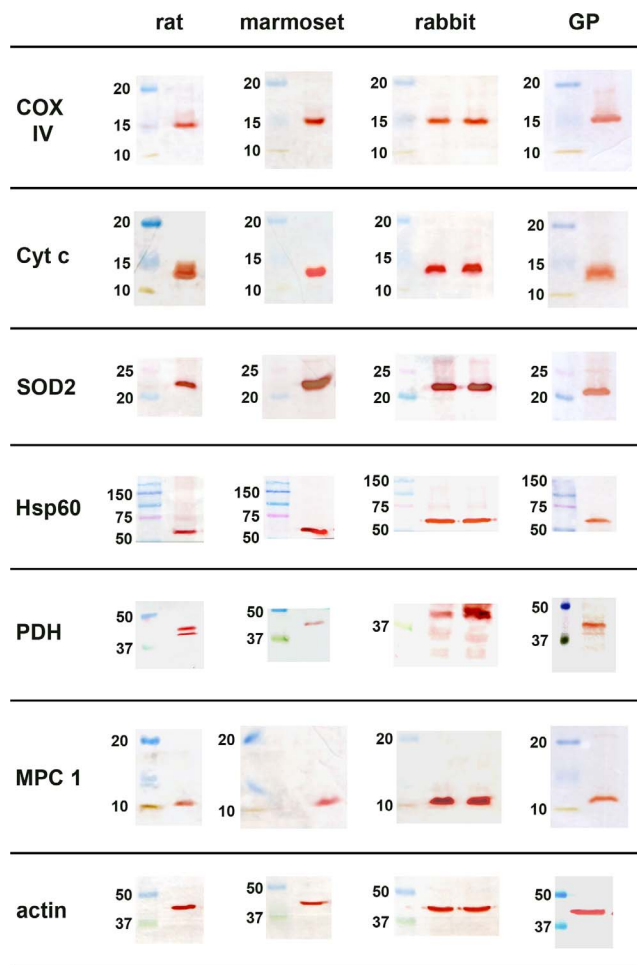
FIGURE 1. Western blot analysis of expression of various mitochondrial proteins in rat, marmoset, rabbit, and guinea pig retinas. Molecular weight markers were used to determine the size of detected gel products. For all proteins analyzed, a major band of the expected molecular weight is apparent, confirming the specificity of each antibody for its intended target in each of the four species. Actin (43 kD); COX IV, cytochrome c oxidase (15 kD); Cyt c, cytochrome c (12 kD); Hsp60, heat shock protein 60 (60 kD); MPC 1, mitochondrial pyruvate carrier 1 (12 kD); PDH, pyruvate dehydrogenase (43 kD); and SOD2, superoxide dismutase 2 (22 kD).

assessed and visually scored on a qualitative scale from '−' (no staining detected) to '+++' (intense staining).

Western Blotting

Tissues were processed for Western blotting as previously described.[21] In brief, entire retinas were dissected and sonicated in homogenization buffer, diluted with an equal volume of sample buffer, and boiled for 3 minutes; protein concentrations in each sample were equalized with the bicinchoninic acid assay. Electrophoresis was performed on 12% denaturing polyacrylamide gels after which proteins were transferred to polyvinylidine fluoride membranes for immunoprobing. Membranes were incubated with the appropriate antisera (as detailed in Table 1), overnight, and labeling carried out using the following multistep detection procedure: first, appropriate biotinylated secondary antibodies were reacted with membranes and then streptavidin-peroxidase conjugates were applied. Blots were developed with a 0.016% solution of 3-amino-9-ethylcarbazole in 50 mM sodium acetate (pH 5)

containing 0.05% Tween-20 and 0.03% H_2O_2. Images were acquired from labeled blots using a Canon CanoLide flatbed scanner (Macquarie Park, New South Wales, Australia).

RESULTS

Validation of Antibodies

Eight mitochondrial proteins were analyzed in the current study. They included COX subunit IV, the last enzyme in the electron transport chain; cytochrome c, the substrate for COX; mitochondrial pyruvate carrier 1 (MPC 1), which facilitates pyruvate transport across the impermeable inner mitochondrial membrane; pyruvate dehydrogenase (PDH), which catalyzes the first step in the conversion of pyruvate into acetyl-CoA; superoxide dismutase-2 (SOD2), which catalyzes the detoxification of superoxide radicals; Hsp60, a mitochondrial chaperone protein; glutamate dehydrogenase, which catalyzes the oxidative deamination of glutamate to α-ketoglutarate, and uMtCK. In order to optimize immunolabeling of antibodies, brain and skeletal muscle tissue sections (see Supplementary Figs. S1A–E for representative images) were used alongside retinal sections. All antibodies employed in the study provided high signal to noise, cell-specific immunolabeling in rat, marmoset, guinea pig, and rabbit sections. No staining was observed in sections in which primary antibody was replaced by isotype/serum controls (Supplementary Figs. 1F–I). By Western blotting, each antibody recognized a discrete, major protein band of the expected molecular weight in retinal extracts from rat, marmoset, rabbit, and guinea pig (Fig. 1). The results further attest to the specificity of the antibodies for use in each species.

Distribution of Mitochondria in Vascular and Avascular Retinas

Inner Retinal Neurons. In the rat, immunoreactivities for COX subunit IV and cytochrome c (Figs. 2A, 2B, 2I, 2J), SOD2 and Hsp60 (Figs. 3A, 3B, 3I, 3J), and MPC 1 and PDH (Figs. 4A, 4B, 4I, 4J) were characterized by intense, punctate labeling of both plexiform layers and the nerve fiber layer. In addition, the somas of larger RGCs were often robustly stained, with moderate labeling evident in the cytoplasm of many cells with the morphologic appearance and location of smaller RGCs, amacrine cells, bipolar cells, and horizontal cells. All of the six proteins displayed similar patterns of labeling, although cytochrome c staining in the inner nuclear layer was particularly strong. As expected, the patterns of mitochondrial labeling in the vascularized marmoset retina (Figs. 2C, 2D, 2K, 2L, 3C, 3D, 3K, 3L, 4C, 4D, 4K, 4L) were highly comparable to those observed in the rat.

In the predominantly avascular rabbit retina, immunoreactivities for COX subunit IV and cytochrome c (Figs. 2E, 2F, 2M, 2N), SOD2 and Hsp60 (Figs. 3E, 3F, 3M, 3N), and MPC 1 and PDH (Figs. 4E, 4F, 4M, 4N) were characterized by weak, but unambiguous, staining of the inner plexiform layer, the inner portion of the outer plexiform layer, and the nerve fiber layer. Of the various cell classes in the inner retina, RGCs were particularly enriched in mitochondrial proteins, a finding that was confirmed by successful colocalization of Hsp60 with the RGC marker RBPMS (Fig. 5). The patterns of mitochondrial labeling in the completely avascular guinea pig retina (Figs. 2G, 2H, 2O, 2P, 3G, 3H, 3O, 3P, 4G, 4H, 4O, 4P) were very similar to those evident in the rabbit. Of interest, staining of RGCs in guinea pig retina was quite striking (see Figs. 2–5).

The rabbit retina, unique among mammals, contains a central band of myelinated nerve fibers, termed the medullary
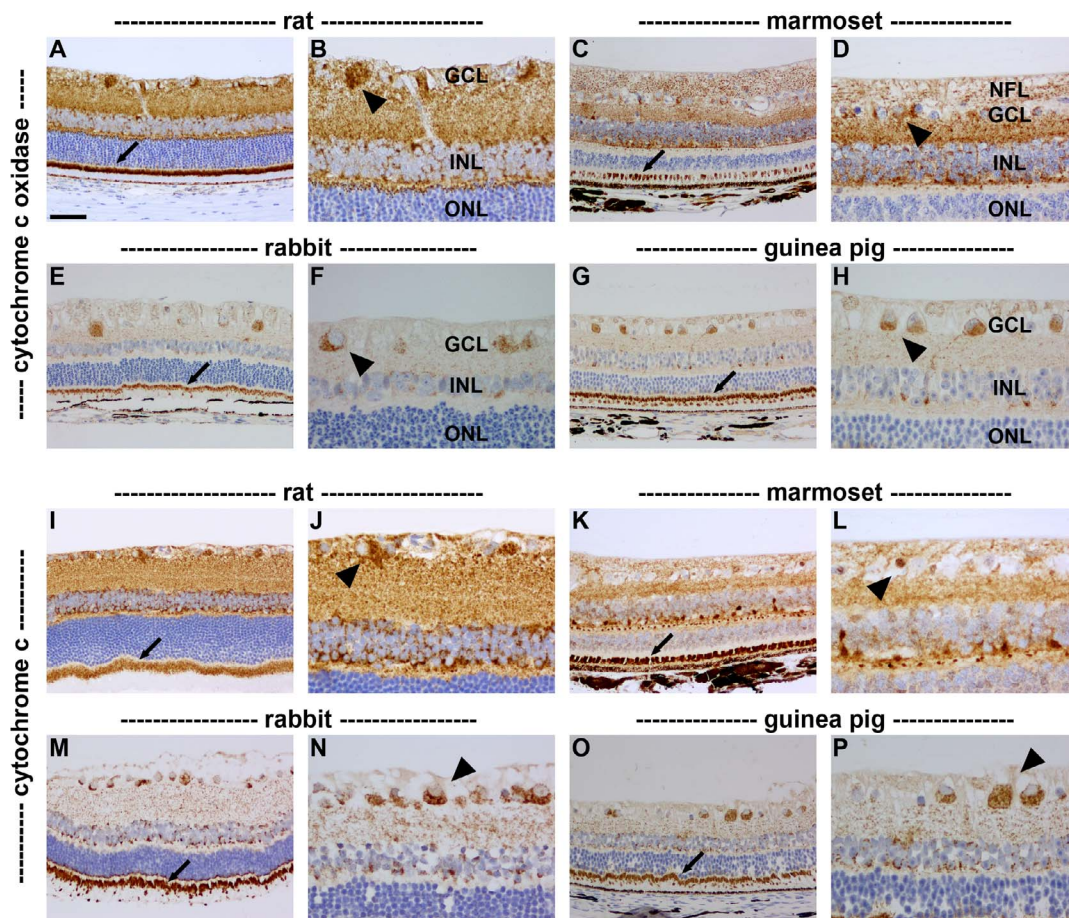
FIGURE 2. Representative images of COX IV and Cyt c immunolabeling in rat, marmoset, rabbit, and guinea pig retinas. Both proteins display comparable patterns of distribution, but the intensities across the various retinal layers vary between vascular and avascular species. In the rat and marmoset, robust labeling of nerve fiber layer, inner and outer plexiform layers, and photoreceptor inner segments (*arrows*) is evident. In the rabbit and guinea pig, intense labeling of photoreceptor inner segments (*arrows*) is apparent, but the inner and outer plexiform layers display only weakly punctate staining. RGC soma labeling is strong in all four species (*arrowheads*). *Scale bar*, (**A, C, E, G, I, K, M, O**) = 50 μm; (**B, D, F, H, J, L, N, P**) = 25 μm. GCL, ganglion cell layer; INL, inner nuclear layer; ONL, outer nuclear layer; NFL, nerve fiber layer.

rays. The majority of the retina is avascular, but a superficial network of capillaries, located between the inner limiting membrane and the nerve fiber layer, exists within the medullary rays. While scrutiny of colorimetric immunolabeling revealed no obvious differences in the distribution patterns of mitochondrial proteins across the retina, we were interested in whether mitochondrial protein expression by RGCs was concentrated within the partially vascularized region of the retina. Thus, we performed double-labeling immunofluorescence of mitochondrial markers both with myelin basic protein (which demarcates myelinated nerve fibers within the medullary rays) and with the vascular endothelial marker CD31. Of importance, the results showed no difference in the expression of mitochondrial proteins between the superficially vascularized and avascular regions of the retina (Fig. 6).

Müller Cells. In order to evaluate immunolabeling of mitochondrial proteins in Müller cells, we focused particularly upon their vitreal endfeet and their scleral-end processes at the external limiting membrane. In addition to the six markers used previously, we also employed an additional mitochondrial marker, glutamate dehydrogenase, which is known to be enriched in glial cells. In rats, and to a lesser extent marmosets, punctate immunolabeling for mitochondrial markers was quite abundant in Müller cell vitreal endfeet abutting the inner limiting membrane, but relatively sparse in their outer stem processes that span the outer nuclear layer and culminate in

scleral-end microvilli (Figs. 2–4, 7). In contrast, in rabbit and guinea pig, no immunolabeling of any mitochondrial marker was observed in their vitreal endfeet, but scleral-end microvilli at the external limiting membrane displayed greater immunoreactivity for mitochondrial markers than vascular retinas (Figs. 5, 7).

Photoreceptors. Immunohistochemical analysis of retinal tissue sections from rat, marmoset, rabbit, and guinea pig incubated with antibodies directed against mitochondrial proteins revealed intense labeling of rod and cone inner segments, but negligible staining of outer segments or photoreceptor somas located in the outer nuclear layer (Figs. 2–4, 8). Overall, the density of mitochondria in the inner segments appeared to be similar in vascular and avascular retinas. All of the six mitochondrial proteins displayed ostensibly identical patterns of expression, although some subtle divergences were evident; for example, in the rat, MPC 1 staining of inner segments was noticeably weaker than that of other mitochondrial proteins. The major difference in photoreceptor mitochondrial distributions in vascular versus avascular retinas was the absence of any punctate labeling of axon terminals in the outer plexiform layer in the avascular rabbit and guinea pig retinas (see also mitochondrial creatine kinase results below).

Retinal Pigment Epithelial (RPE). Positive immunolabeling for mitochondrial proteins was observed in the RPE of rat,
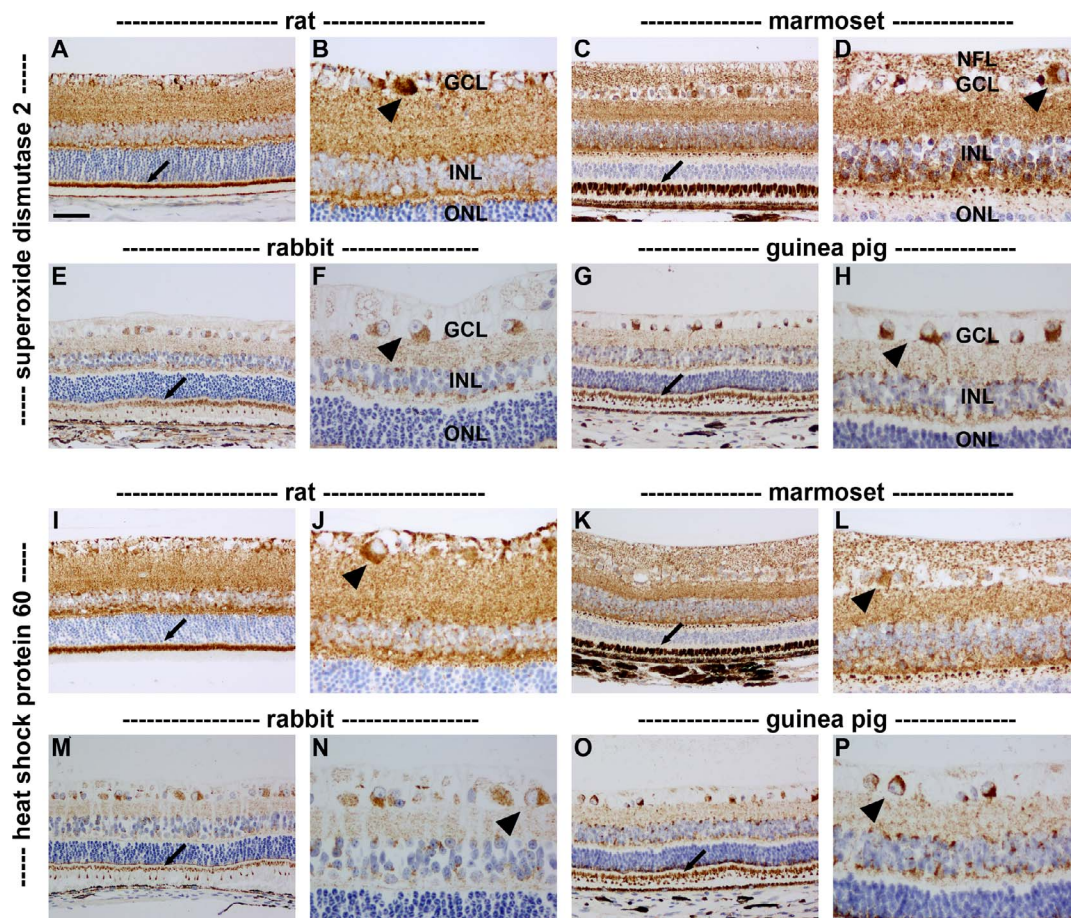
FIGURE 3. Representative images of superoxide dismutase 2 and heat shock protein 60 immunolabeling in rat, marmoset, rabbit, and guinea pig retinas. Both proteins display analogous patterns of distribution, but the intensities across the various retinal layers vary between vascular and avascular species. In the rat and marmoset, strong labeling of nerve fiber layer, inner and outer plexiform layers, and photoreceptor inner segments (*arrows*) is apparent. In the rabbit and guinea pig, intense staining of photoreceptor inner segments (*arrows*) is apparent, but the inner and outer plexiform layers display weaker punctate labeling. RGC soma labeling is compelling in all four species (*arrowheads*). *Scale bar*, (**A**, **C**, **E**, **G**, **I**, **K**, **M**, **O**) = 50 μm; (**B**, **D**, **F**, **H**, **J**, **L**, **N**, **P**) = 25 μm.

marmoset, rabbit, and guinea pig (Fig. 8). In all four species, mitochondria were enriched at the basolateral surface of this monolayer. There was no readily identifiable difference in intensity of staining between vascular and avascular retinas.

Activity of Mitochondria in Vascular and Avascular Retinas

To complement the results of the immunohistochemistry experiments, we performed enzyme histochemistry assays for three mitochondrial enzymes (COX, SDH, and ICDH) using unfixed retinal sections. These assays provide spatial information pertaining to mitochondrial activity: retinal layers with high mitochondrial activity present high assay activity. COX, SDH, and ICDH displayed equivalent patterns of intensity to each other, but their activities varied across the different species. Thus, in the rat, highest activity of each enzyme was observed in photoreceptor inner segments, with high activity also observed in both plexiform layers, and lowest activity in the outer nuclear layer and outer segments (Figs. 9A, 9D, 9G). In the rabbit and guinea pig, similar levels of mitochondrial activity were seen in photoreceptor inner segments to those observed in the rat, but activities in both the inner and outer plexiform layers were substantially lower. Moderate activity could be discerned in putative Müller cell scleral-end processes near the external limiting membrane and in individual

mitochondria of RGCs of both the rabbit and guinea pig (Figs. 9B, 9C, 9E, 9F, 9H, 9I).

Semiquantitative Grading of Mitochondrial Immunolabeling and Activity in Vascular and Avascular Retinas

In order to make some tentative inferences about the relative abundance and activity of mitochondria in the different layers of vascular and avascular retinas, we devised a rudimentary, semiquantitative grading scheme to evaluate the immunostaining and enzyme histochemistry data. The overall results are summarized in Table 2. There are obvious caveats to any conclusions drawn; for example, immunohistochemistry is not a technique inherently suited to quantification of proteins levels. Moreover, when used for the purposes of cross-species comparison, the unknown affinities of each antiserum for its target protein in the different species becomes confounding. Furthermore, not all mitochondrial proteins labeled in an identical fashion within the same species. Nevertheless, the results do provide a useful overview of the distribution and activity of mitochondria in vascular and avascular retinas, highlighting similarities (inner segments, RPE) and differences (inner retinal neurons, polarized distribution of mitochondria in Müller cells).
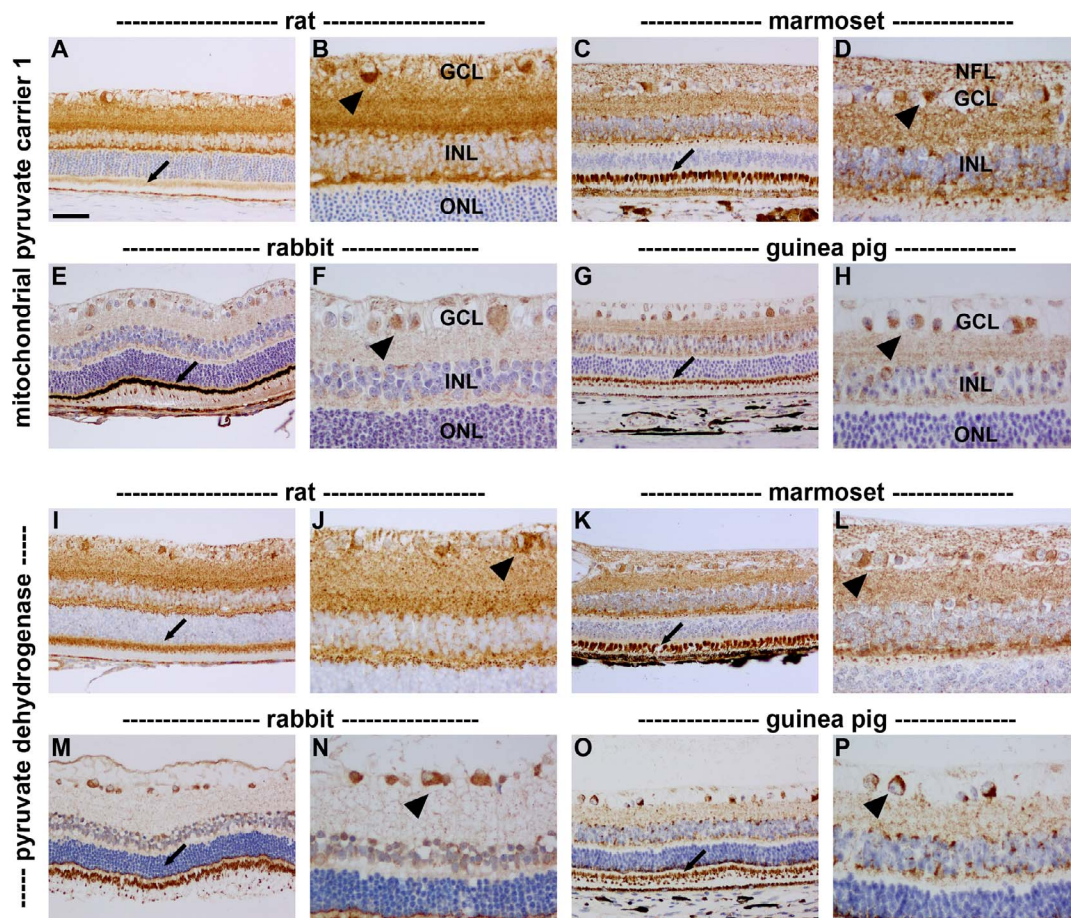
FIGURE 4. Representative images of mitochondrial pyruvate carrier 1 and pyruvate dehydrogenase immunolabeling in rat, marmoset, rabbit, and guinea pig retinas. Both proteins display similar patterns of distribution, but the intensities across the various retinal layers vary between vascular and avascular species. In the rat and marmoset, strong labeling of nerve fiber layer, inner and outer plexiform layers, and photoreceptor inner segments (*arrows*) is evident. In the rabbit and guinea pig, intense staining of photoreceptor inner segments (*arrows*) is apparent, but the inner and outer plexiform layers display weak punctate labeling, particularly the rabbit. RGC soma labeling is unambiguous in all four species (*arrowheads*). *Scale bar*, (**A, C, E, G, I, K, M, O**) = 50 μm; (**B, D, F, H, J, L, N, P**) = 25 μm.

Mitochondrial Creatine Kinase in Vascular and Avascular Retinas

UMtCK converts creatine to phosphocreatine, providing energy buffering in cells with varying energy requirements. By Western blotting, the uMtCK antibody recognized a major protein band
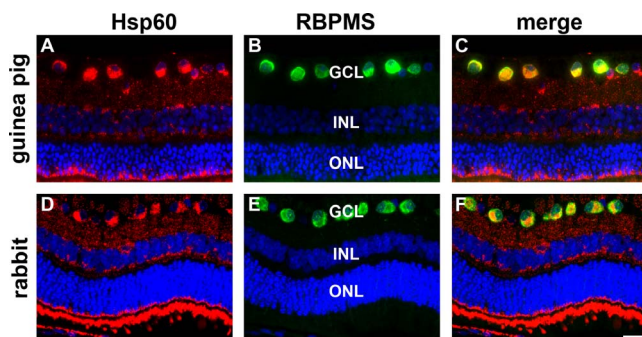

FIGURE 5. Double-labeling immunofluorescence of mitochondrial markers in the rabbit and guinea pig retina. (**A–C**) In the guinea pig retina, the mitochondrial marker Hsp60 (*red*) colocalizes with RBPMS (*green*) in RGCs. (**D–F**) In the rabbit retina, Hsp60 (*red*) similarly colocalizes with RNA-binding protein with multiple splicing (RBPMS) (*green*). *Scale bar*, (**A–F**) 20 μm.

of the expected molecular weight in retinal extracts of rat, marmoset, and rabbit (Fig. 10A). The distribution patterns of uMtCK in rat, marmoset, rabbit, and guinea pig retinas (Figs. 10B–I) were fundamentally similar, with labeling restricted to neuronal populations, most notably rod and cone photoreceptors and RGCs (Table 3). As expected, labeling of both plexiform layers was more intense in the vascular retinas, but, interestingly, uMtCK immunoreactivity in the inner plexiform layer of the rabbit and guinea pig was stronger than for any of the other mitochondrial proteins analyzed in these species (Table 3). Photoreceptor terminals, visualized using the presynaptic marker synaptophysin, were positive for uMtCK in rat (Figs. 10J, 10K) and marmoset, but not in rabbit and guinea pig (Figs. 10L, 10M), attesting to the polarized distribution of mitochondria in photoreceptors of avascular retinas. Double-labeling immunofluorescence experiments of uMtCK with the Müller cell marker S100 or with the ubiquitous mitochondrial chaperone protein Hsp60 revealed that uMtCK (unlike Hsp60) was not detectable in Müller cell endfeet, somas, or scleral-end processes in either vascular or avascular retinas (Fig. 11).

Distribution of Mitochondria in Mouse Retina

To complement the results obtained in rat, we also performed some limited investigations into the distribution of mitochondria in the vascularized mouse retina (Fig. 12). The overall
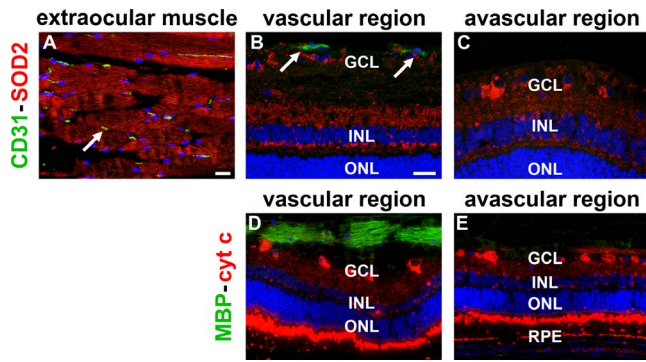
FIGURE 6. Double-labeling immunofluorescence of mitochondrial markers in the vascular and avascular regions of the rabbit retina. (**A**) Representative image of the vascular endothelial marker CD31 (*green, arrow*) double labeled with SOD2 (*red*) in rabbit extraocular muscle. (**B**) SOD2 immunoreactivity (*red*) in the inner rabbit retina is present within the superficially vascularized central zone of the retina, which is demarcated by CD31-positive capillaries (*green, arrows*). (**C**) SOD2 immunoreactivity is detectable to an equivalent degree within the completely avascular majority of the retina that does not feature CD31 immunoreactivity. (**D**) Cyt c immunoreactivity (*red*) in the inner retina is present within the superficially vascularized central zone of the retina termed the medullary rays, which is characterized by myelinated nerve fibers that are positive for myelin basic protein (*green*). (**E**) Cyt c immunoreactivity is detectable to an equivalent degree within the completely avascular majority of the retina that does not feature myelinated axons. *Scale bars*, 30 μm. MBP, myelin basic protein.

results revealed that the mouse displays patterns of immuno-labeling that are essentially identical to the rat, including intense staining of inner segments and both plexiform layers, robust labeling of larger RGCs, positive immunolabeling of Müller cell vitreal endfeet, and polarized expression of mitochondrial proteins in RPE. As in the rat, uMtCK expression in the ganglion cell layer of the mouse was particularly intense.

DISCUSSION

The first conclusion to be drawn from the present study is that the distributions of mitochondria in mammalian species that possess either vascular or avascular retinas are not as divergent as might be expected from knowledge of the respective oxygen availabilities. In avascular retinas, mitochondria encompass the inner layers of the retina, notably RGCs (see Table 2). The data confirm and extend the findings of Germer and colleagues[10,11] and Stone et al.,[12] who demonstrated immunolabeling for GABA transaminase and COX, respectively, within RGCs of rabbit and guinea pig retinas. The results are likewise consistent with an earlier study that investigated the activities of various enzymes of energy metabolism in the different layers of the mudpuppy retina.[22] The mudpuppy retina is also an avascular structure that depends on the choroid for its oxygen and nutrient supply. The most logical explanation for the failure of Bentmann et al.[9] to identify cytochrome c in the inner retina of the guinea pig relates to a lack of sensitivity of their immunohistochemical assay.

To complement the immunohistochemistry data, we performed in situ enzyme histochemistry assays for three critical mitochondrial enzymes involved in the tricarboxylic acid cycle and electron transport chain, ICDH, SDH, and COX. Imaging of reactions in unfixed tissue sections permits evaluation of enzyme activities in a manner faithful to the in vivo situation,[23] assuming that an inert polymer, such as polyvinyl alcohol, is included in the incubation medium as a tissue protectant to prevent diffusion of soluble macromolecules.[24] The mitochondrial matrix enzyme ICDH, for example, is highly diffusible. All three enzyme assays yielded similar results, which closely resembled the protein distribution patterns elicited by immunolabeling. Our findings in the rat retina are in complete agreement with the results of previous reports describing COX activity in vascularized rat,[25,26] mouse,[27] and human[28] retinas. To our knowledge, in situ enzyme histochemistry has not previously been performed in avascular retinas. The results showed that rabbit and guinea pig displayed ostensibly identical patterns of enzyme activity to
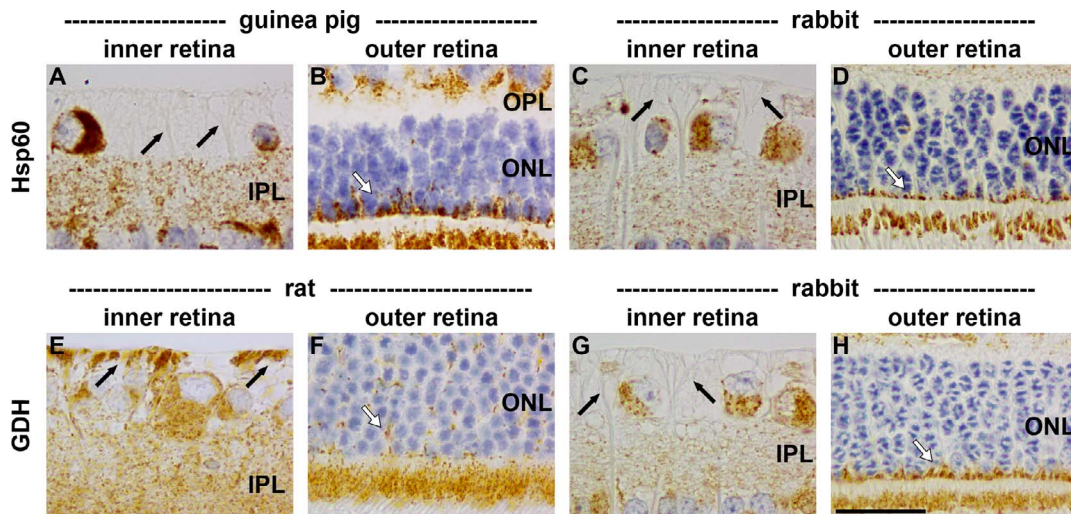

FIGURE 7. Representative images of Hsp60 (**A–D**) and glutamate dehydrogenase (**E–H**) immunolabeling in Müller cells of vascular and avascular retinas. In the avascular guinea pig and rabbit retina, Hsp60 is not expressed by Müller cell end-feet at the vitreal surface (*black arrows* [**A**, **C**]). In contrast, Hsp60 immunoreactivity is present within Müller cell end feet at the external limiting membrane (*white arrows* [**B**, **D**]). In the vascular rat retina, glutamate dehydrogenase (GDH) is detectable throughout Müller cell processes (*black and white arrows* [**E**, **F**]). Conversely, in the avascular rabbit retina, GDH immunoreactivity is only evident within Müller cell scleral end processes at the external limiting membrane (*black and white arrows* [**G**, **H**]). *Scale bar*, 10 μm.
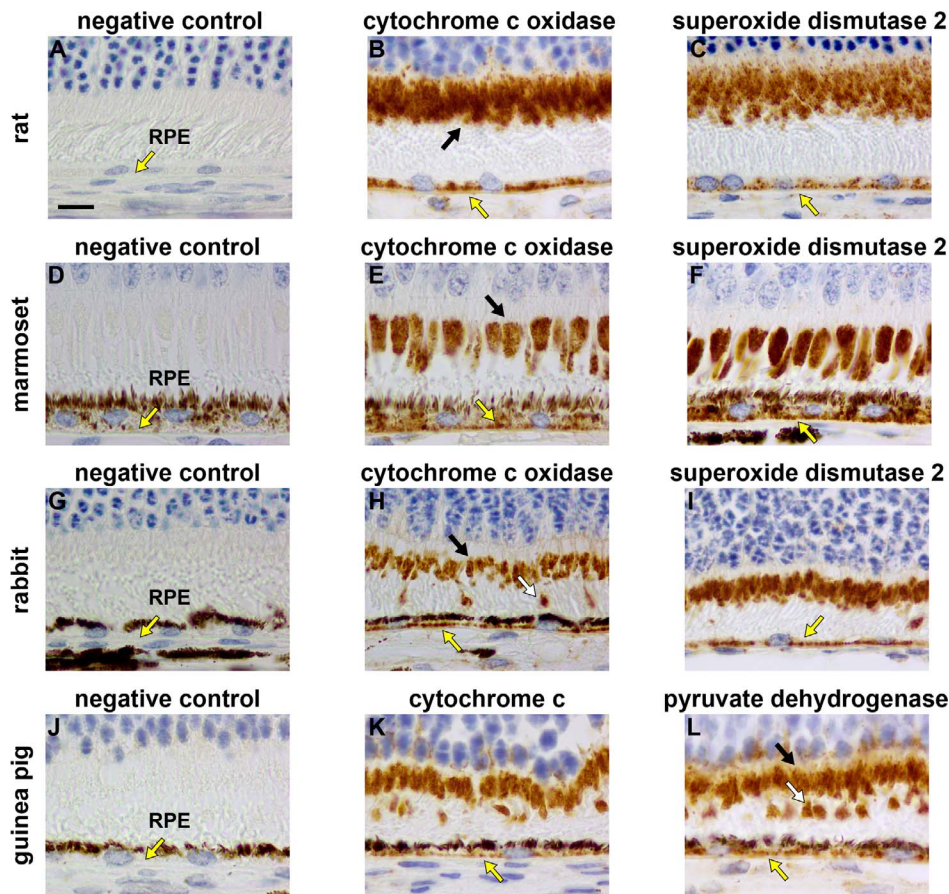
FIGURE 8. Representative images of mitochondrial immunolabeling in rat (**A–C**), marmoset (**D–F**), rabbit (**G–I**), and guinea pig (**J–L**) photoreceptor segments and RPE. In all four species, mitochondrial proteins (cyt c oxidase, SOD2, and cyt c) are concentrated in rod (*black arrows*) and cone (*white arrows*) inner segments and at the basolateral surface of the RPE (*yellow arrows*). The presence of melanin pigment partly confounds interpretation of staining in the RPE of the marmoset, rabbit, and guinea pig, but comparison with negative control (minus primary) tissue sections reveals specific staining. *Scale bar*, 10 μm.

each other and confirm that functional mitochondria reside within the innermost layer of the avascular retina, farthest from the choriocapillaris.

The most notable difference between the intensities of mitochondrial proteins/enzyme activities in the avascular as opposed to vascular retinas was the considerably weaker reactions observed in the inner and outer plexiform layers of the avascular species. Mitochondria were not absent from the plexiform layers in the rabbit and guinea pig, but both their expression and activity were sparse when compared with the rat and marmoset. The plexiform layers feature synaptic connections between dendrites and axons of different neuronal classes. They have high energy demands to facilitate neurotransmission and maintenance of membrane potential. In the vascularized rat retina, modelling has shown that, alongside photoreceptor inner segments, the outer plexiform layer and the deeper region of the inner plexiform layer are the dominant oxygen-consuming layers.[5] The high oxygen usage of both plexiform layers matches the high-enzyme activities documented in this study. Conversely, in both rabbit and guinea pig, modelling has shown that oxygen consumption in the inner retina is remarkably low, in the guinea pig being less than 6% of the outer retina.[5] One explanation for the low oxygen usage in the outer plexiform layer of avascular retinas is that mitochondria are lacking from photoreceptor axon terminals, in contrast to the vascularized retina where they are prevalent.[12] Our data provide robust support for this

conclusion. We found no colocalization of mitochondrial markers with the presynaptic marker synaptophysin in rabbit or guinea pig.

On the whole, the vascularized rat and marmoset retinas displayed very similar patterns of mitochondrial distribution. This is to be expected given their similar oxygen profiles across the retinal layers.[5,29] While we were unable to source human retinas, previous studies investigating mitochondria in human retina have found comparable patterns of expression to those of monkey and rat, with highest abundance observed in photoreceptor inner segments, high levels noted in the plexiform layers and nerve fiber layer, and unequivocal labeling of RGCs and the RPE.[10,12,28,30]

A crucial function of mitochondria in tissues, such as the retina, which have prodigious as well as variable, energy requirements is the generation of high-energy phosphocreatine from creatine and ATP, via the action of uMtCK. Phosphocreatine, which is stable and highly diffusible, then acts as a temporal and spatial energy buffer within the cell.[31] The presence of uMtCK within rod and cone inner segments has previously been demonstrated in chick and mouse retinas.[27,32–34] Experimental evidence supports the existence of a phosphocreatine shuttle within photoreceptors from the inner segments to terminals situated in the outer plexiform layer when energy demand is high during darkness,[32] and to outer segments during the light.[33] Herein, we observed abundant uMtCK expression in the inner segments of all four
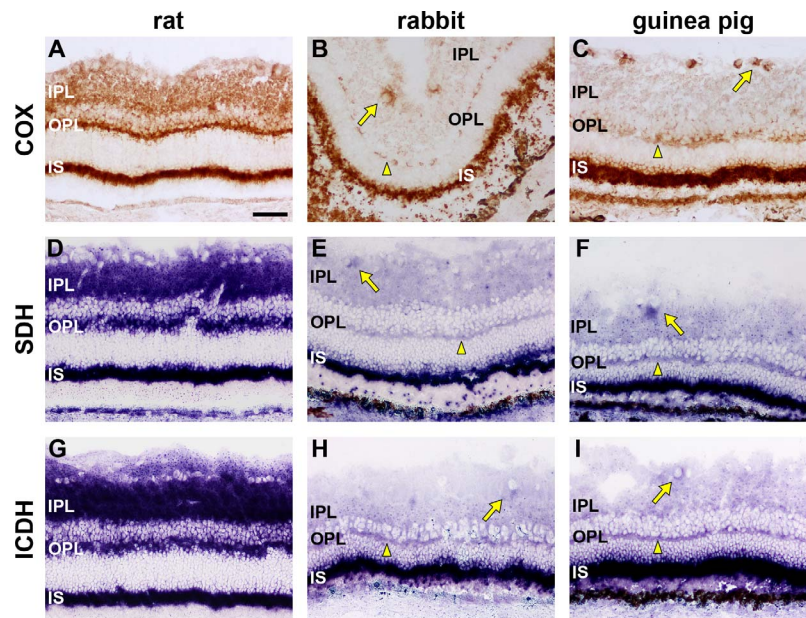
FIGURE 9. Representative images of COX (**A–C**), SDH (**D–F**), and ICDH (**G–I**) activities in rat, rabbit, and guinea pig retinas. All three mitochondrial enzyme activities (COX, SDH, and ICDH) display equivalent patterns of intensity to each other across the various retinal layers, but their activities vary between species. In the rat, highest activity of each enzyme is observed in photoreceptor inner segments, with both plexiform layers also robustly labeled. Relatively little enzyme activity is observed in the cytoplasm surrounding the nuclei of the ONL, with higher reactivity localized to cells of the INL, and strong reactivity within mitochondria of retinal ganglion cells. In the rabbit and guinea pig, similar levels of activity of each enzyme are seen in photoreceptor inner segments to that observed in the rat, but activities in both the inner and outer (*arrowhead*) plexiform layers are markedly lower. Moderate activity could frequently be discerned in mitochondria of retinal ganglion cells of both the rabbit and guinea pig (*arrows*) and in Müller cell scleral end processes. *Scale bar*, 50 μm. IS, inner segments.

species. Of note, however, uMtCK was absent from photoreceptor terminals in the rabbit and guinea pig, supporting the assertion by Linton et al.[32] that photoreceptor terminals in avascular retinas, which are devoid of mitochondria, are dependent upon a flux of phosphocreatine from the inner segments. To date, the role of phosphocreatine in the inner retina has received little attention. Two notable findings are evident from the present study. Firstly, uMtCK was strongly expressed in RGCs of rabbit and guinea pig, with weak to moderate expression in the inner plexiform layer. Of all of the mitochondrial proteins analyzed, uMtCK displayed the strongest labeling in avascular retinas. Of course, direct comparison of the levels of expression of different proteins is not reliable by immunohistochemistry and the strong labeling may simply reflect optimal assay conditions; however, it is reasonable to postulate that RGCs utilize uMtCK to generate a large cellular store of phosphocreatine when oxygen tension permits. Certainly, the presence of uMtCK within the inner layers of avascular retinas supports the concept of the functional relevance of these mitochondria. The second key finding was that uMtCK was not detectable in Müller cells in any of the four species investigated, a result that concurs precisely with the cellular distribution of uMtCK in the mouse brain, where it is abundantly expressed in neurons, but is not detectable in glial cells.[15] The lack of uMtCK in Müller cells is also consistent with the observation that Müller cells lack creatine transporters.[35] It can be concluded that a phosphocreatine flux exists in neuronal, but not in glial, mitochondria, reflecting the greater oxidative metabolism of neurons.

Notwithstanding the absence of uMtCK in Müller cells, all of the other mitochondrial proteins analyzed yielded patterns of immunolabeling that were consistent with their presence in this cell type. In the rat, marmoset, and mouse, Müller cells contained mitochondria throughout their length, but in the rabbit and guinea pig, mitochondria were only evident at the

scleral-end processes nearest to the choriocapillaris. This was particularly evident when labeling for glutamate dehydrogenase, which is known to be enriched in Müller cells.[36] The results mirror those of Germer and colleagues,[10,11] who studied expression of GABA transaminase.

An unambiguous finding of our study is that mitochondrial proteins are enriched at the basolateral membrane of the RPE, an observation consistent across all four species analyzed as well as mouse. The results correspond precisely with those of Stone et al.,[12] who showed by electron microscopy that mitochondria congregate at the basal surface of RPE cells in avascular wallaby and vascular human retinas. The suggested explanation for this polarized distribution is simply proximity to the choriocapillaris. A number of recent studies have highlighted the critical role of mitochondria within RPE cells, both in terms of maintaining a healthy intracellular environment and in allowing RPE cells to sustain adjacent photoreceptors.[37–41]

Overall, our results indicate that RGCs, and to a lesser extent all inner retinal neurons, in the rabbit and guinea pig likely undergo oxidative phosphorylation; they are not entirely dependent upon anerobic glycolysis. This is not unexpected for the rabbit, because oxygen tension—while low within the ganglion cell layer when compared with measured values in vascularized retinas—is nonetheless of the order of 10 mm Hg.[5,42] In the guinea pig, however, oxygen tension is close to zero.[5,6] Yet, the patterns of immunolabeling and enzyme activities were analogous in both species. In fact, RGCs arguably stained more intensely for mitochondrial proteins in the guinea pig. Moreover, there was no discernible difference in the expression of mitochondrial proteins between the partially vascularized central region of the rabbit retina and the avascular majority of the retina, a finding that matches data showing that any flux of oxygen to the inner retina from a vitreal route is negligible.[5] It appears likely that the additional

TABLE 2. Semiquantitative Grading of Mitochondrial Immunolabeling and Activity

| Retinal Layer | Vascular (Rat and Marmoset) | | Avascular (Rabbit and Guinea Pig) | |
	Labeling Intensity	Enzyme Activity	Labeling Intensity	Enzyme Activity
GCL	++	++	++	+/++
IPL	+++	+++	+	+
INL neurons	+/++	++	+	+
Müller cell (vitreal)	+/++	+	−	−
Müller cell (scleral)	+	++	+/++	++
OPL	+++	+++	+	+/++
ONL	−	−	−	−
Inner segments	+++	+++	+++	+++
Outer segments	−	−	−	−
RPE	++	++	++	++

Grading scheme: − = minimal labeling, + = weak labeling, ++ = moderate labeling, +++ = intense labeling.

TABLE 3. Semiquantitative Grading of Mitochondrial Creatine Kinase Immunolabeling

Retinal Layer	Vascular (Rat and Marmoset) Labeling Intensity	Avascular (Rabbit and Guinea Pig) Labeling Intensity
GCL	++/+++	++/+++
IPL	++/+++	+/++
INL neurons	+/++	+
Müller cell (vitreal)	−	−
Müller cell (scleral)	−	−
OPL	++/+++	+
ONL	−	−
Inner segments	+++	+++
Outer segments	−	−
RPE	−	−

Grading scheme: − = minimal labeling, + = weak labeling, ++ = moderate labeling, +++ = intense labeling.
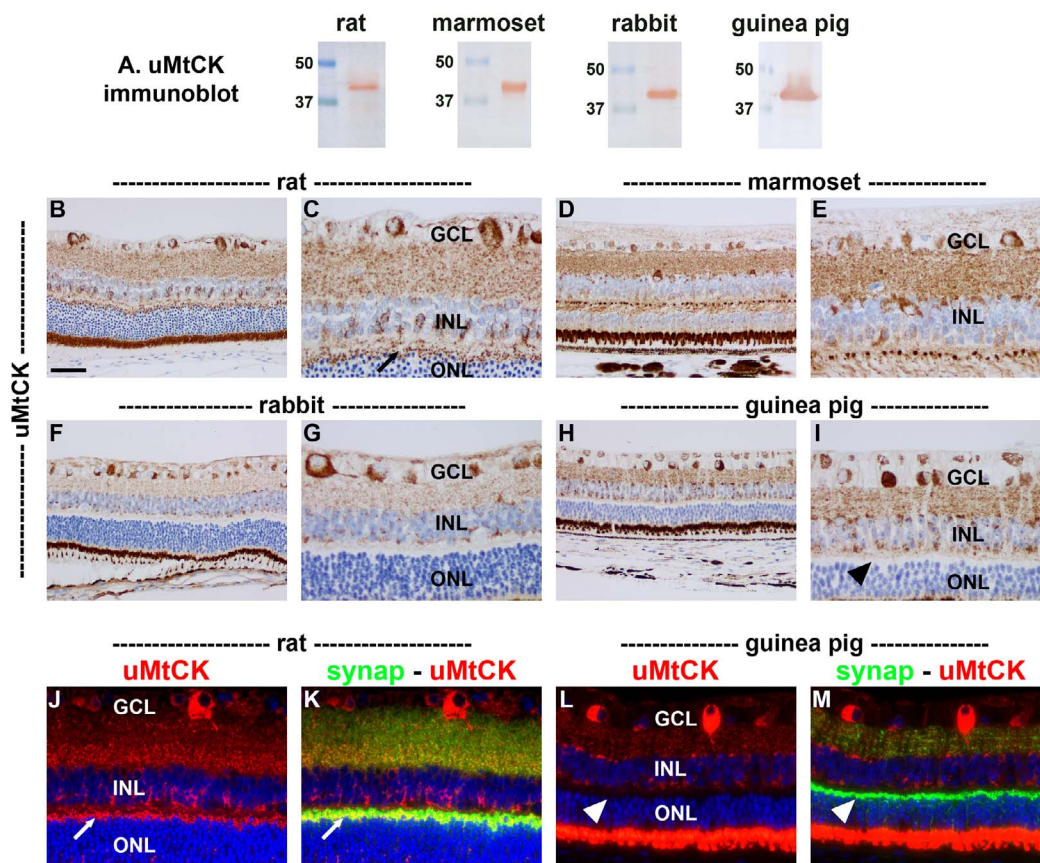

FIGURE 10. Representative Western blot and immunohistochemical analysis of expression of ubiquitous mitochondrial creatine kinase in rat, marmoset, and rabbit retina. (**A**) Western blot analysis of ubiquitous mitochondrial creatine kinase. Molecular weight markers were used to determine the size of detected gel products. For each species, a major band of the expected molecular weight (40 kD) is apparent, confirming the specificity of each antibody for its intended target. (**B–M**) Images of uMtCK immunolabeling in vascular and avascular retinas. uMtCK displays comparable staining patterns in all four retinas, featuring labeling of the nerve fiber layer, RGCs, the inner and outer plexiform layers, and photoreceptor inner segments. RGCs are strongly positive in all four species. Double-labeling immunofluorescence of uMtCK (*red*) with the presynaptic marker synaptophysin (*green*) reveals that colocalization of these proteins is observed within photoreceptor synapses in the distal portion of the outer plexiform layer in the rat (*arrow*), but not in the guinea pig (*arrowhead*). *Scale bars*, (**B**, **D**, **F**, **H**) = 50 μm; (**C**, **E**, **G**, **H**, **I**) = 25 μm; (**J–M**) = 20 μm.
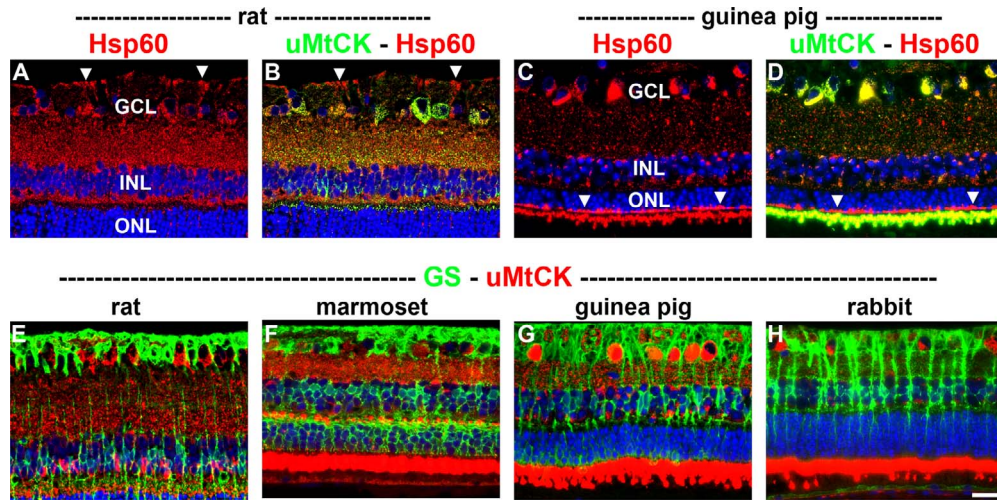
FIGURE 11. Lack of expression of uMtCK by Müller cells in vascular and avascular retinas. (**A–D**) Double-labeling immunofluorescence of the ubiquitous mitochondrial chaperone protein Hsp60 (*red*) with uMtCK (*green*) reveals a lack of colocalization within Müller cell vitreal endfeet in rat ([**A**, **B**] *arrowheads*) and Müller cell scleral-end processes at the outer limiting membrane in guinea pig ([**C**, **D**] *arrowheads*). (**E–H**) Double-labeling immunofluorescence of uMtCK (*red*) with the Müller cell marker S100 (*green*) shows no unambiguous colocalization within Müller cell processes or somas in any of the four species. *Scale bar*, 20 μm.

oxygen provided by the superficial vessels within the medullary rays is effectively negligible, at least in terms of facilitating greater oxidative phosphorylation in the plexiform layers. Different theories can be postulated to account for the relative abundance of mitochondria within RGCs of the avascular retina. One possible explanation relates to the presence of neuroglobin, an oxygen-binding haem protein expressed by neurons.[43] Initial studies reported that neuroglobin was abundantly expressed within vascular[44] and avascular[9] retinas, and that a proportion of the protein localized to mitochondria where it acted as an oxygen supply

protein facilitating respiratory chain function.[45] Subsequent work, however, has led to reappraisal both of the level of expression and the distribution of neuroglobin in the retina.[46,47] It is now believed that the protein is restricted to a subset of RGCs and amacrine cells in the murine retina, while the distribution in avascular retinas remains to be determined. It is questionable whether neuroglobin is expressed sufficiently within the avascular retina that it could play a central role in oxygen homeostasis and energy metabolism; nevertheless, given its putative expression by RGCs of the avascular retina, it is certainly conceivable it could play a role in sequestering
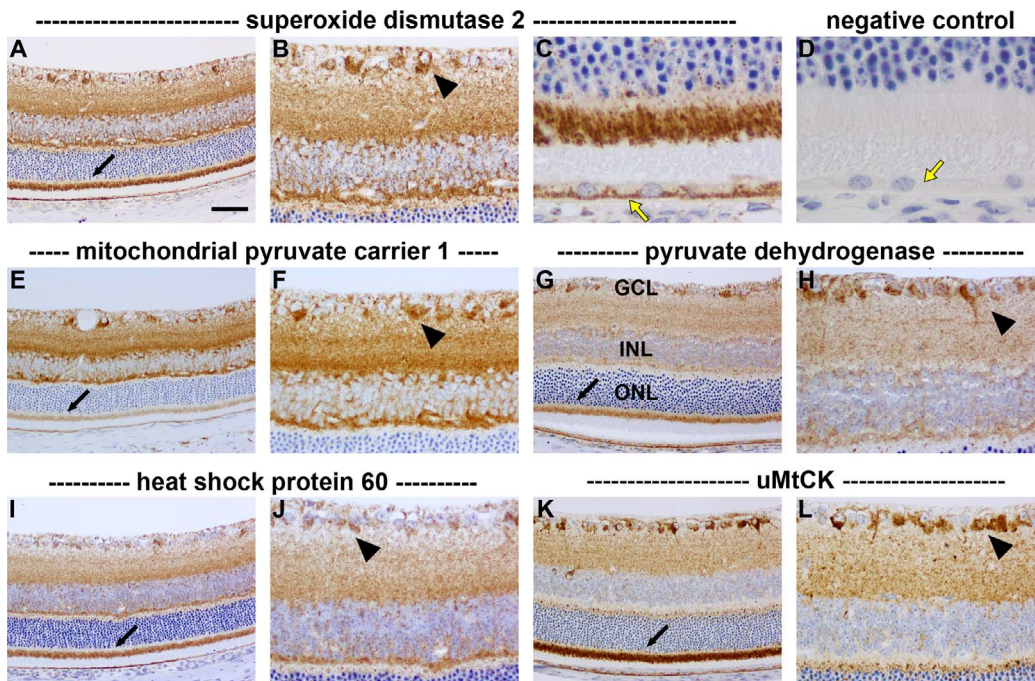

FIGURE 12. Representative images of mitochondrial immunolabeling in mouse retina. All five mitochondrial proteins display similar patterns of distribution featuring robust labeling of the inner and outer plexiform layers, and photoreceptor inner segments (*black arrows*). RGCs are enriched with mitochondrial proteins (*arrowheads*). In the RPE, mitochondrial proteins are prominent at the basolateral surface (*yellow arrow*). *Scale bar*, (**A, E, G, I, K**) = 50 μm; (**B, F, H, J, L**) = 25 μm; (**C, D**) = 10 μm.

oxygen in these cells. A second and more pragmatic explanation for the presence of mitochondria within the avascular innermost retina was put forward by Yu and Cringle[5] who proposed that there exists a very precise matching of retinal oxygen consumption with choroidal oxygen supply across the retina. In conclusion, the current findings advance our understanding of the metabolic similarities and differences between vascular and avascular retinas, and underscore the idea that RGCs in the avascular rabbit and guinea pig are not entirely dependent upon anerobic glycolysis.

Acknowledgments

References

1. Anderson B Jr, Saltzman HA. Retinal oxygen utilization measured by hyperbaric blackout. *Arch Ophthalmol*. 1964; 72:792–795.

2. Puchowicz MA, Xu K, Magness D, et al. Comparison of glucose influx and blood flow in retina and brain of diabetic rats. *J Cereb Blood Flow Metab*. 2004;24:449–457.

3. Kur J, Newman EA, Chan-Ling T. Cellular and physiological mechanisms underlying blood flow regulation in the retina and choroid in health and disease. *Prog Retin Eye Res*. 2012; 31:377–406.

4. Chase J. The evolution of retinal vascularization in mammals. A comparison of vascular and avascular retinae. *Ophthalmology*. 1982;89:1518–1525.

5. Yu DY, Cringle SJ. Oxygen distribution and consumption within the retina in vascularised and avascular retinas and in animal models of retinal disease. *Prog Retin Eye Res*. 2001;20: 175–208.

6. Yu DY, Cringle SJ, Alder VA, Su EN, Yu PK. Intraretinal oxygen distribution and choroidal regulation in the avascular retina of guinea pigs. *Am J Physiol*. 1996;270:H965–H973.

7. Lowry OH, Roberts NR, Schulz DW, Clow JE, Clark JR. Quantitative histochemistry of retina. II. Enzymes of glucose metabolism. *J Biol Chem*. 1961;236:2813–2820.

8. Country MW. Retinal metabolism: a comparative look at energetics in the retina. *Brain Res*. 2017;1672:50–57.

9. Bentmann A, Schmidt M, Reuss S, Wolfrum U, Hankeln T, Burmester T. Divergent distribution in vascular and avascular mammalian retinae links neuroglobin to cellular respiration. *J Biol Chem*. 2005;280:20660–20665.

10. Germer A, Biedermann B, Wolburg H, et al. Distribution of mitochondria within Muller cells–I. Correlation with retinal vascularization in different mammalian species. *J Neurocytol*. 1998;27:329–345.

11. Germer A, Schuck J, Wolburg H, Kuhrt H, Mack AF, Reichenbach A. Distribution of mitochondria within Muller cells–II. Post-natal development of the rabbit retinal periphery in vivo and in vitro: dependence on oxygen supply. *J Neurocytol*. 1998;27:347–359.

12. Stone J, van Driel D, Valter K, Rees S, Provis J. The locations of mitochondria in mammalian photoreceptors: relation to retinal vasculature. *Brain Res*. 2008;1189:58–69.

13. Wallimann T, Tokarska-Schlattner M, Schlattner U. The creatine kinase system and pleiotropic effects of creatine. *Amino Acids*. 2011;40:1271–1296.

14. Rae CD, Broer S. Creatine as a booster for human brain function. How might it work? *Neurochem Int*. 2015;89:249–259.

15. Tachikawa M, Fukaya M, Terasaki T, Ohtsuki S, Watanabe M. Distinct cellular expressions of creatine synthetic enzyme GAMT and creatine kinases uCK-Mi and CK-B suggest a novel neuron-glial relationship for brain energy homeostasis. *Eur J Neurosci*. 2004;20:144–160.

16. Collins MG, Rogers NM, Jesudason S, Kireta S, Brealey J, Coates PT. Spontaneous glomerular mesangial lesions in common marmoset monkeys (Callithrix jacchus): a benign non-progressive glomerulopathy. *J Med Primatol*. 2014;43: 477–487.

17. Chidlow G, Daymon M, Wood JP, Casson RJ. Localization of a wide-ranging panel of antigens in the rat retina by immuno-histochemistry: comparison of Davidson's solution and formalin as fixatives. *J Histochem Cytochem*. 2011;59:884–898.

18. Chidlow G, Wood JP, Casson RJ. Expression of inducible heat shock proteins hsp27 and hsp70 in the visual pathway of rats subjected to various models of retinal ganglion cell injury. *PLoS One*. 2014;9:e114838.

19. Chidlow G, Wood JP, Knoops B, Casson RJ. Expression and distribution of peroxiredoxins in the retina and optic nerve. *Brain Struct Funct*. 2016;221:3903–3925.

20. Shaw PJ. Comparison of widefield/deconvolution and confo-cal microscopy for three-dimensional imaging. In: Pawley J, ed. *Handbook of Biological Confocal Microscopy*. New York: Springer US; 2006:453–467.

21. Chidlow G, Holman MC, Wood JP, Casson RJ. Spatiotemporal characterization of optic nerve degeneration after chronic hypoperfusion in the rat. *Invest Ophthalmol Vis Sci*. 2010;51: 1483–1497.

22. Dick E. Enzymes of energy metabolism in the mudpuppy retina. *J Neurochem*. 1984;43:1124–1131.

23. Van Noorden CJF, Frederiks WM. Metabolic mapping by enzyme histochemistry. In: Kiernan JA, Mason I, eds. *Microscopy and Histology for Molecular Biologists*. London: Portland Press; 2002:277–311.

24. Van Noorden CJ, Vogels IM. Polyvinyl alcohol and other tissue protectants in enzyme histochemistry: a consumer's guide. *Histochem J*. 1989;21:373–379.

25. Chen E, Soderberg PG, Lindstrom B. Activity distribution of cytochrome oxidase in the rat retina. A quantitative histo-chemical study. *Acta Ophthalmol*. 1989;67:645–651.

26. Kageyama GH, Wong-Riley MT. The histochemical localization of cytochrome oxidase in the retina and lateral geniculate nucleus of the ferret, cat, and monkey, with particular reference to retinal mosaics and ON/OFF-center visual channels. *J Neurosci*. 1984;4:2445–2459.

27. Rueda EM, Johnson JE Jr, Giddabasappa A, et al. The cellular and compartmental profile of mouse retinal glycolysis, tricarboxylic acid cycle, oxidative phosphorylation, and ∼P transferring kinases. *Mol Vis*. 2016;22:847–885.

28. Andrews RM, Griffiths PG, Johnson MA, Turnbull DM. Histochemical localisation of mitochondrial enzyme activity in human optic nerve and retina. *Br J Ophthalmol*. 1999;83: 231–235.

29. Yu DY, Cringle SJ, Su EN. Intraretinal oxygen distribution in the monkey retina and the response to systemic hyperoxia. *Invest Ophthalmol Vis Sci*. 2005;46:4728–4733.

30. Hoang QV, Linsenmeier RA, Chung CK, Curcio CA. Photo-receptor inner segments in monkey and human retina: mitochondrial density, optics, and regional variation. *Vis Neurosci*. 2002;19:395–407.

31. Wallimann T, Wyss M, Brdiczka D, Nicolay K, Eppenberger HM. Intracellular compartmentation, structure and function of creatine kinase isoenzymes in tissues with high and fluctuating energy demands: the 'phosphocreatine circuit' for cellular energy homeostasis. *Biochem J*. 1992;281(Pt 1):21–40.

32. Linton JD, Holzhausen LC, Babai N, et al. Flow of energy in the outer retina in darkness and in light. *Proc Natl Acad Sci U S A*. 2010;107:8599–8604.

33. Wallimann T, Wegmann G, Moser H, Huber R, Eppenberger HM. High content of creatine kinase in chicken retina: compartmentalized localization of creatine kinase isoenzymes in photoreceptor cells. *Proc Natl Acad Sci U S A*. 1986;83:3816–3819.

34. Wegmann G, Huber R, Zanolla E, Eppenberger HM, Wallimann T. Differential expression and localization of brain-type and mitochondrial creatine kinase isoenzymes during development of the chicken retina: Mi-CK as a marker for differentiation of photoreceptor cells. *Differentiation*. 1991; 46:77–87.

35. Acosta ML, Kalloniatis M, Christie DL. Creatine transporter localization in developing and adult retina: importance of creatine to retinal function. *Am J Physiol Cell Physiol*. 2005; 289:C1015–C1023.

36. Gebhard R. Histochemical demonstration of glutamate dehydrogenase and phosphate-activated glutaminase activities in semithin sections of the rat retina. *Histochemistry*. 1992;97:101–103.

37. Lefevere E, Toft-Kehler AK, Vohra R, Kolko M, Moons L, Van Hove I. Mitochondrial dysfunction underlying outer retinal diseases. *Mitochondrion*. 2017;36:66–76.

38. He Y, Tombran-Tink J. Mitochondrial decay and impairment of antioxidant defenses in aging RPE cells. *Adv Exp Med Biol*. 2010;664:165–183.

39. Terluk MR, Kapphahn RJ, Soukup LM, et al. Investigating mitochondria as a target for treating age-related macular degeneration. *J Neurosci*. 2015;35:7304–7311.

40. Rohrer B, Bandyopadhyay M, Beeson C. Reduced metabolic capacity in aged primary retinal pigment epithelium (RPE) is correlated with increased susceptibility to oxidative stress. *Adv Exp Med Biol*. 2016;854:793–798.

41. Mao H, Seo SJ, Biswal MR, et al. Mitochondrial oxidative stress in the retinal pigment epithelium leads to localized retinal degeneration. *Invest Ophthalmol Vis Sci*. 2014;55:4613–4627.

42. Tillis TN, Murray DL, Schmidt GJ, Weiter JJ. Preretinal oxygen changes in the rabbit under conditions of light and dark. *Invest Ophthalmol Vis Sci*. 1988;29:988–991.

43. Burmester T, Hankeln T. Function and evolution of vertebrate globins. *Acta Physiol (Oxf)*. 2014;211:501–514.

44. Schmidt M, Giessl A, Laufs T, Hankeln T, Wolfrum U, Burmester T. How does the eye breathe? Evidence for neuroglobin-mediated oxygen supply in the mammalian retina. *J Biol Chem*. 2003;278:1932–1935.

45. Lechauve C, Augustin S, Cwerman-Thibault H, et al. Neuroglobin involvement in respiratory chain function and retinal ganglion cell integrity. *Biochim Biophys Acta*. 2012;1823: 2261–2273.

46. Hundahl CA, Fahrenkrug J, Luuk H, Hay-Schmidt A, Hannibal J. Restricted expression of Neuroglobin in the mouse retina and co-localization with Melanopsin and Tyrosine Hydroxylase. *Biochem Biophys Res Commun*. 2012;425:100–106.

47. Fabrizius A, Andre D, Laufs T, et al. Critical re-evaluation of neuroglobin expression reveals conserved patterns among mammals. *Neuroscience*. 2016;337:339–354.